



TAMPEREEN TEKNILLINEN YLIOPISTO
TAMPERE UNIVERSITY OF TECHNOLOGY

JANI PATRAKKA
THERMOACTUATED TWIST IN LIQUID CRYSTAL
ELASTOMER FOR TEMPERATURE SENSING

Bachelor's thesis

Tampere, September 13, 2017

TIIVISTELMÄ

JANI PATRAKKA: Lämpötilan havaitseminen nestekide-elastomeerin lämpöherätteen kiertymän avulla

Tampereen Teknillinen Yliopisto

Kandidaatintyö, 3+36 sivua

13. syyskuuta 2017

Teknis-luonnontieteellinen koulutusohjelma

Pääaine: Teknillinen fysiikka

Tarkastaja: Professori Arri Priimägi

Ohjaaja: Tohtori Hao Zeng

Avainsanat: nestekide, nestekide-elastomeeri, lämpöherätteen, lämpötilan havaitseminen, relaksaatioaika, ristosilloitus, sensori, termoaktuaatio

Tämä kandidaatintyö tarkastelee mahdollisuutta soveltaa nestekide-elastomeerejä lämpötilaa havaitsevissa sensoreissa. Materiaalin lämpöominaisuuksien tutkimiseksi nestekide-elastomeeristä valmistettiin valopolymeroimalla ohut kalvo sopivan molekulaarisen järjestyksen mukaisesti, ja kalvosta leikattiin tutkittava kaistale elastomeeriä, kiertynyt nauha. Nauha asetettiin roikkumaan lämpötilasäädeltävään mittauskammioon, josta nauhan kärjen kiertymää lämpötilan muuttuessa voitiin tarkastella järjestelmäkameran avulla. Materiaalin lämpötilaherkkyys mitattiin ja sitä verrattiin markkinoilla saatavilla oleviin nestekiteisiin perustuviin lämpömittareihin mahdollisen sensorin mittaustarkkuuden määrittämiseksi. Sen jälkeen nauhan kärjen kiertymän kulman muutos karakterisoitiin lämpötilan funktiona käyttäen kolmea eri lämpötilagradienttia. Lisäksi nauhan relaksaatioaika nopean lämpötilan muutoksen jälkeen mitattiin vakio­lämpötilassa.

Nauhan lämpötilan muutoksen erotuskyvyn todettiin olevan $0,1\text{ }^{\circ}\text{C}$. Mittaustulokset osoittivat, että lämpötilagradientti ja sitä vastaava kulmamuutos eli myös suurin kulmamuutos ovat käänteisesti riippuvaisia tietyllä lämpötilavälillä: lämpötilan muutoksella $2\text{ }^{\circ}\text{C}/\text{min}$ kulmamuutokseksi saatiin $36\text{ }^{\circ}/\text{K}$, kun taas lämpötilan muutos $0,5\text{ }^{\circ}\text{C}/\text{min}$ johti noin $40\text{ }^{\circ}/\text{K}$ kulmamuutokseen. Relaksaatioajaksi vakio­lämpötilassa mitattiin $\tau = 150\text{ min}$. Suurin mitattu kulma relaksaatioajan mittauksessa ylitti kuitenkin muiden mittausten perusteella johdetun mallin mukaisen arvion, kenties johtuen mittauksessa käytetystä yli kaksi kertaluokkaa muiden mittausten lämpötilagradientteja nopeammasta lämpötilan muutoksesta. Tutkimuksen tulokset vaikuttavat kuitenkin lupaavilta lämpötilaa havaitsevan sensorisovelluksen kannalta, sillä toistettavuus oli huomattavaa ja uskomme pystyvämme parantamaan laitteen mittaustarkkuutta yli kymmenkertaisesti. Jatkotutkimus kohdistuu materiaalin lämpötilaherkkyiden parantamiseen sekä lämpötilagradientin vaikutusten tutkimiseen.

ABSTRACT

JANI PATRAKKA: Thermoactuated twist in liquid crystal elastomer for temperature sensing

Tampere University of Technology

Bachelor's thesis, 3+36 pages

September 13, 2017

Bachelor's Degree Programme in Science and Engineering

Major: Physics

Examiner: Prof. Arri Priimägi

Advisor: Dr. Hao Zeng

Keywords: crosslinking, liquid crystal, liquid crystal elastomers, relaxation time, sensor thermoactuation, thermal sensing

This thesis explores the possibility of utilising liquid crystal elastomers (LCE) for thermal sensing applications. To measure its thermal properties, a thin film of LCE was photopolymerised in splayed nematic alignment and cut out to form a helical shape, a coil. The coil was then set within a temperature-controlled measurement compartment and observed through a camera setup as the tip of the coil twisted upon heating or cooling. Thermal sensitivity of the coil was subsequently measured and compared to other LC-based thermal sensing systems to assess the sensor's thermal resolution. This angular change of the twist was then characterised as a function of temperature with three temperature gradients. In addition, the relaxation time of the coil was measured in constant temperature after rapid heating and cooling.

Thermal resolution of the coil is reported to be $0,1\text{ }^{\circ}\text{C}$. The results of the research also indicate an inverse relation between the temperature gradient and the maximum angle as well as the angular change per degree of temperature measured at a certain temperature range: for a temperature gradient of $2\text{ }^{\circ}\text{C}/\text{min}$, the angular change was measured to be $36\text{ }^{\circ}/\text{K}$, whereas a gradient of $0,5\text{ }^{\circ}\text{C}/\text{min}$ yielded an angular change of $40\text{ }^{\circ}/\text{K}$. Relaxation time of the material in a constant temperature proved to be $\tau = 150\text{ min}$. Maximum angles in the relaxation time measurement exceeded the expected values based on an experimental model derived from the other measurements, possibly due to the temperature gradient over two orders of magnitude greater. The results show great promise in a thermal sensor application with good reproducibility and potential for improving the thermal resolution over tenfold in the future. Further research is needed to optimise the thermal sensitivity of the material as well as to study the effect of temperature gradient on angular change of the coil.

CONTENTS

1. Introduction	2
2. Theory and background	3
2.1 Liquid crystals	3
2.1.1 Order parameter	5
2.1.2 Liquid crystal domains	6
2.1.3 Nematic, smectic and cholesteric phases	7
2.2 Liquid crystal elastomers	9
2.3 Thermoactuated deformation	10
2.3.1 Molecular alignment	10
2.3.2 Thermal sensitivity	12
2.3.3 Adding some twist to it	13
2.4 Applications	14
3. Sample preparation and methods	17
3.1 Preparing the sample	17
3.2 Experimental setup	19
3.2.1 Determining the relaxation time	21
3.2.2 Measuring the sensitivity	21
3.3 Processing the data	22
4. Results and Discussion	23
4.1 Relaxation time	23
4.2 Measurements of angular change	25
5. Conclusions	32
References	34

LIST OF ABBREVIATIONS AND SYMBOLS

LC	Liquid crystal
LCD	Liquid crystal display
LCE	Liquid crystal elastomer
LCN	Liquid crystal network
SNA	Splayed nematic alignment
TUT	Tampere University of Technology
\vec{n}	Director vector of preferential alignment
T_m	Phase transition point between solid and liquid crystal phases
T_c	Clearing point, i.e. phase transition point between liquid crystal and liquid phases
S	Order parameter
τ	Relaxation time

1. INTRODUCTION

Of all the nature's wonders, liquid crystals are admittedly one of its most fascinating aspects. Somewhere between solid and liquid lies a phase with properties of both as well as some properties neither of the aforementioned possess. Although these properties enable a vast variety of applications ranging from consumer electronics to experimental photonics and microrobotics, they also provide liquid crystals with something perhaps even more precious, namely their uniquely beautiful texture. It may have been just that what Friedrich Reinitzer, a young Austrian botanist in the late 19th century, found so irresistibly intriguing when he discovered a strange phase of certain cholesterol derivatives we nowadays refer to as cholesteric phase liquid crystals. [1]

Reinitzer unlikely comprehended the true meaning of his discovery nor that researchers over a century later would write about his findings as an introduction to various publications. However, the phase of matter he brought into the open continues to enthral still. To fully appreciate liquid crystals and their remarkable features, one must understand the phenomena related to the uniqueness of liquid crystals (LC) as well as their elastic polymer chains, liquid crystal elastomers (LCE).

This thesis delves into the mysteries of liquid crystals, liquid crystal elastomers and their applications to explore the possibility of devising a thermal sensor from liquid crystal elastomers. The first chapter of the thesis deals with the physics making the sensor possible, followed by a chapter regarding liquid crystal elastomer sample preparation and description of the measurement setup. The last two chapters are dedicated to measurement results and their analysis, and summary and future outlook, respectively.

So — what is needed in order to build a thermal sensor with a liquid crystal elastomer?

2. THEORY AND BACKGROUND

In order to understand the fundamental phenomena that make thermal sensor applications with LCE materials possible, a brief overview of the physics of LCs, LCEs and the properties of material that enable thermoactuated deformation is presented. After introducing the concept of thermoactuated deformation in LCEs, some potential applications of the phenomenon are presented.

2.1 Liquid crystals

There exist materials that demonstrate an intermediate phase with properties similar to both liquid and solid phases. These materials, *liquid crystals* (LC), exhibit liquid crystal phases within a temperature range $T_m < T < T_c$ intrinsic to the material, where T_m is the transition temperature between crystalline solid and LC phase and T_c the clearing point after which the material melts into an isotropic liquid. As illustrated by an example LC molecule in Fig. 2.1, these typically rod-like molecules exhibit partial orientational order to some specific direction in LC phases due to intermolecular interactions but no rigid crystalline structure and thus no positional order found in solids. This combination gives rise to remarkable features such as *anisotropic* materials properties, combined with high molecular mobility as in liquids.

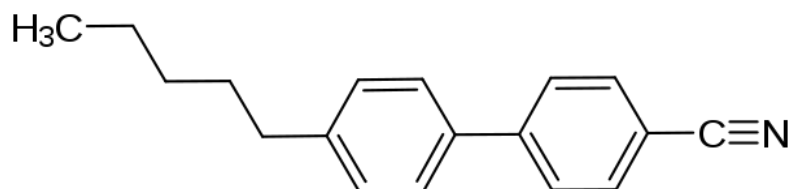


Figure 2.1 *4-Cyano-4'-pentylbiphenyl molecule.* Better known as 5CB, the commonly rod-shaped molecule exhibits nematic liquid crystal phase in room temperature.

In this thesis, anisotropy is defined by having asymmetric material properties as a function of direction. In other words, unlike isotropic materials, anisotropic materials evince different mechanical, optical and dielectric properties when probed from different directions. This implies, for example, that light propagating from one direction with a certain polarisation will interact with the material differently as opposed to light propagating from a different direction or with a different polarisation. These asymmetric interactions occur only below the isotropic phase transition temperature, whereupon material's isotropic liquid properties dominate light-matter interactions. [1]

Lacking positional order, typically rod-shaped molecules in LCs can move past each other due to thermal motion similarly as in a liquid. The molecules' uniaxial orientation along their longitudinal axis, denoted as z-axis, is displayed in Fig. 2.2. This type of condensed matter with some molecular orientational order but without the long-range periodical order of a crystalline solid has the appearance of a cloudy liquid. [2] Due to anisotropy, several optical properties can be observed in liquid crystals including *birefringence* and *dichroism*. Various liquid crystal phases can be observed with polarised light given the anisotropic nature of the material. [3]

Anisotropic materials in LC phase with orientational order along one symmetry axis are uniaxially birefringent. [4] Birefringence is defined by the refractive index of an anisotropic material being dependent on the polarisation and propagation direction of the incident light. The phenomenon can be observed in a birefringent LC: a beam of light propagating through the material is divided into two beams of different polarisation with respect to the symmetry axis on the material. Consequently, birefringence is present in anisotropic materials with more than one symmetry axis but the phenomenon is far more complex.

Another optical property emerging from the partial orientational order of the material is dichroism. [5] Materials with absorbance varying as a function of polarisation of incident light are considered dichroic. This optical property can be utilised in various applications ranging from camrecorders and LCD projectors to decorative objects.

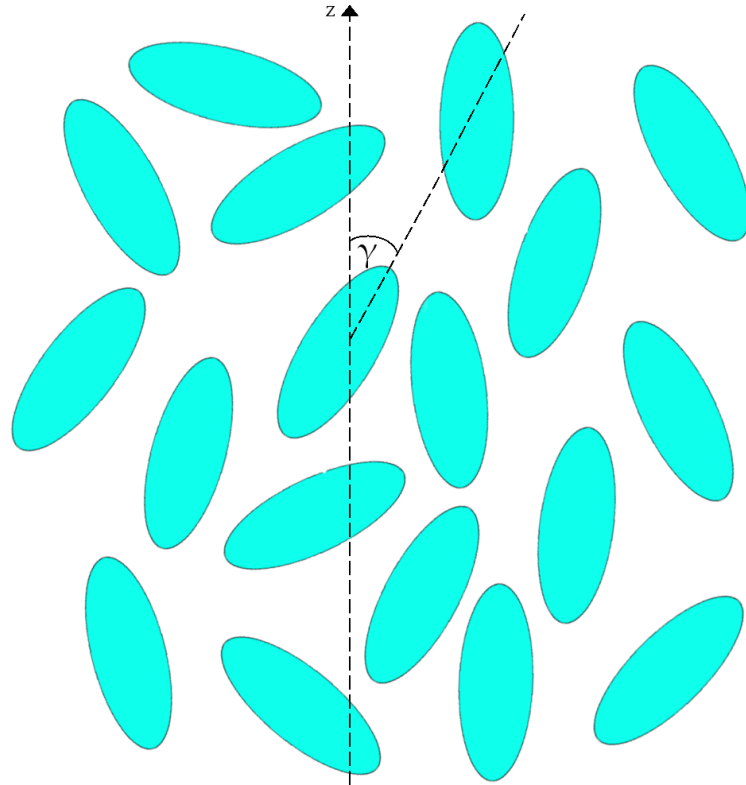


Figure 2.2 Orientation of molecules in a liquid crystal. Illustration of molecules at any given moment in the LC along the preferred orientation director z with individual molecule's angle to the director γ , where $0^\circ < \gamma < 90^\circ$.

Liquid crystals behave distinctively in response to temperature. Below the phase transition temperature T_m , the material remains fully solid in a crystalline form. This temperature is always below material's clearing point T_c after which a phase transition to isotropic liquid occurs. However, between these two temperatures exist the LC phases. [1]

2.1.1 Order parameter

Below the isotropic phase transition temperature, LC molecules within a certain region in the material are partially orientated along the same director \vec{n} which gives rise to optical properties characteristic to different LC phases. The dimensionless unit vector \vec{n} is used to describe material anisotropy by denoting the preferred orientation of adjacent LC molecules and thus parallel to their average longitudinal axes. The director can be externally controlled with high precision using electric fields or physical alignment layers, yielding various applications such as electrically operated LC displays [6]. This partial orientational order can be represented with

the *order parameter* S , in its exact form a second-order symmetric tensor used to quantitatively describe the degree of order within the material. [7] This thesis, however, deals with uniaxial nematic liquid crystals where the molecules have one director along a preferred axis with rotational symmetry around the axis and hence a simple scalar order parameter, where $0 < S < 1$, suffices:

$$S = \left\langle \frac{3 \cos^2(\gamma) - 1}{2} \right\rangle, \quad (2.1)$$

where γ is the angle of the molecule to the preferred alignment and S is averaged. Calculating numerous γ for a selection of LC molecules, the average angle and thus orientational order can be determined: LCs with an average angle below 57° have partial orientational order. The order parameter can be measured empirically from birefringence or polarized absorption spectra, for example. [7]

2.1.2 Liquid crystal domains

Using a polarised microscope, distinct *domains* can be observed within the structure. Within the domains, adjacent LC molecules are locally uniformly orientated. Molecules in different domains, however, can be orientated along different directors. Entirely uniform LC is called *monodomain* LC. Materials' monodomain LC properties can be verified by observing these domains through a polarising microscope while rotating the sample.

In polarised optical microscopy (POM), a microscope includes two polarisers referred to as *polariser* near the light source and *analyser* near the camera sensor. [4] Between the polarisers is a space for the sample to be analysed. The polariser and analyser are aligned so that their polarisation is perpendicular. Lacking an electric field component in parallel with the analyser's polarisation, the linearly polarised light from the first polariser cannot propagate through the analyser onto the camera sensor within the microscope, resulting in a black image. With a birefringent material in between, however, light interacts with the matter and modulates the polarization, hence forming an image.

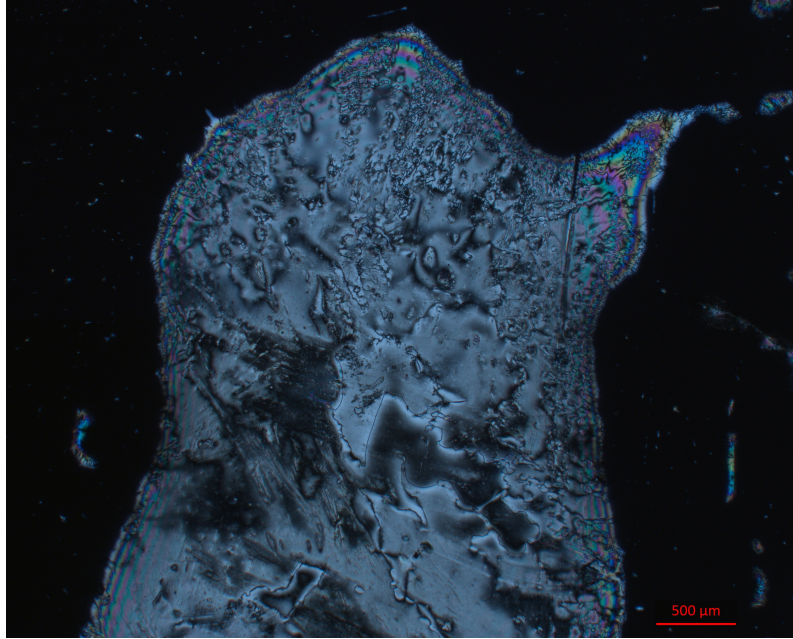


Figure 2.3 *Polarising microscope image of LC monomer mixture E7. A drop of E7 liquid crystal mixture at room temperature. Dark areas represent light through the glass substrate without interaction with the droplet.*

In Fig. 2.3, the image of an E7 LC mixture droplet was taken with the microscope's polarisers crossed. The glass substrate without any LC on it, shown here as the black area surrounding the droplet, is dark due to the light polarised at the first polariser being blocked by the analyser. Similarly, the dark areas within the droplet exhibit domains where the director is in parallel with the polariser and thus the electric field of the incident light. Therefore the polarisation of the light is not modulated by the LC molecules and the analyser becomes impermeable to most of the illumination. The brighter areas, however, contain LC domains with the director with an angle to the electric field of the polarised light. The domains visible in the image polarise light along the second optical filter's polarisation angle to a greater extent thus providing a brighter image of the LCE. [8]

2.1.3 Nematic, smectic and cholesteric phases

Between material-specific T_m and T_c temperatures, LCs evidence a variety of phases, such as *nematic*, *smectic* and *cholesteric* phases. For the purpose of this thesis, the nematic phase is the most relevant. In the nematic phase, molecules are mainly uniaxially orientated along their longitudinal axis, depending on the degree of long-range orientational order in the material, but exhibit no positional order as their centers of mass are in liquid-like random motion. The molecules with an angle to the director are referred to as *disclinations*. [1] The molecules' freedom to move

past each other within the LC structure enables low-energy molecular realignment crucial to plethora of applications discussed in more detail in section 2.4.

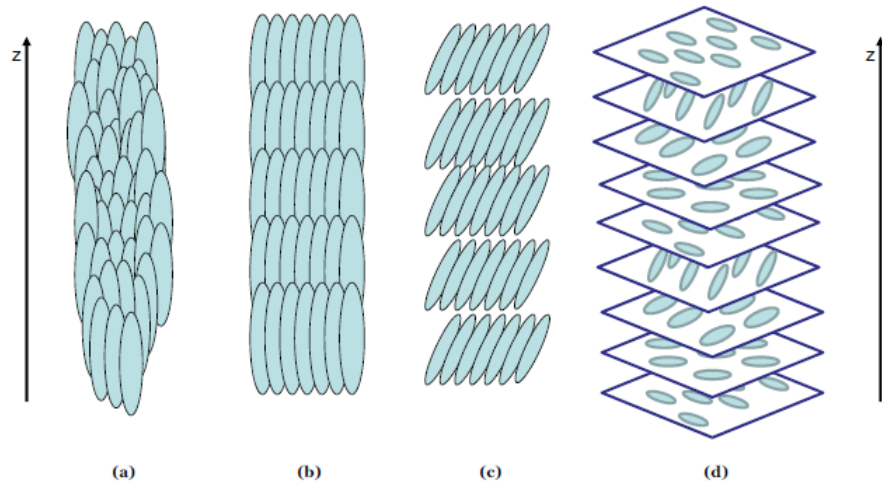


Figure 2.4 Most common Liquid crystal (LC) phases. (a) nematic phase, (b) smectic A phase, (c) smectic C phase, (d) cholesteric phase. [9]

Most common LC phases are presented in Fig. 2.4. When cooled down sufficiently, some nematic liquid crystals exhibit extraordinary behaviour indicating another phase. This phase is called *smectic phase* because its constitution resembles soapy materials. Unlike in nematic phase, the molecules in smectic phases display translational order by aligning in layers as depicted in Fig. 2.4 (b) and (c). In this smectic alignment, several separate types can be distinguished with smectic A and smectic C types being most common. These phases differ by director's angle with respect to the layers' normal vector. [10] Similarly to nematic phase, however, the LC molecules in smectic A phase are orientated in the direction of the layers' normal vector denoted in Fig. 2.4 as z axis while in smectic C phase the molecules are with an angle to the z .

If the LC orientation rotates symmetrically around the z -axis in a helical fashion as shown in Fig. 2.4 (d), the liquid crystal is in cholesteric or chiral nematic phase. For the cholesteric phase, the director of the orientation depends on the angle of the twist of the helical structure. The distance between two layers with the same director is known as (*chiral*) *pitch*. More specifically, pitch is the distance in which the angle of the director changes 360° . While 180° twist results in two layers of molecules with parallel directors, this distance is only half a pitch. Chiral pitch is significant for optical applications of cholesteric phase LCs as it results in a high degree of reflection of incident irradiation of equal wavelength and thus altering the pitch effectively changes the wavelength, a unique property applied in low-threshold laser emission systems as well as thermal sensors, for example. [11]

2.2 Liquid crystal elastomers

An *elastomer* is, by definition, an elastic polymer with two key features: viscosity and elasticity. Viscosity determines the solid rubber-like structure of the material while elasticity, defined as the material's capacity to recover its original shape and configuration after stretching, due to weak inter-molecular Van der Waals forces permits the polymer chains to move past each other as the material is elongated. This feature is highly beneficial for LC materials capable of molecular realignment actuated by external electric field, magnetic field or illumination as realignment in LC phases often results in elongation or contraction. [8]

Due to the extremely versatile applications of elastic polymers, various polymerisation mechanisms have been developed. [12] Step-growth polymers can be based on condensation reactions in polymerisation by merging two monomers and consequently eliminating some small molecule, usually H_2O , in the process. Another mechanism for step-growth polymers involves addition reactions utilising unsaturated monomers' double or triple carbon bonds to merge monomers, while chain-growth polymers are generally formed in the presence of *free radicals* in a three-stage process. [8]

The first stage of the polymerisation, chain initiation, involves the formation of free radicals through electron transfer or single bond severance. After the free radicals attack the monomers' bonds and thus facilitate their merging, the propagation stage begins. The final stage entails chain transfer or termination of the free radicals, effectively finishing the polymerisation step.[8] One example of free radical polymerisation is *photopolymerisation* resulting in chain-growth polymers through light-initiated reactions. [13] Absorbing light of suitable wavelength can occur directly in the monomers, for example liquid crystal molecules, in which case the reaction is direct photopolymerisation, whereas light absorbed by a dopant and subsequently transferred to the monomer is indirect. Both mechanisms are frequently employed in 3D printing, for example.

With long polymer chains within the elastomer, returning to its original shape after relieving elongating stress on the material would be unlikely without *crosslinking*. Although some materials exhibit elasticity without covalent crosslinking but rather through thermodynamic mechanisms, most elastomers rely on bonds between polymer chains. These links make the structure more rigid and provide the basis for the material's elastic reversion to pre-stressed shape. [8] Crosslinking provides the material with 'elastic memory' in terms of reversion: cross-links ensure that two connected points on adjacent chains realign similarly as prior to material deforma-

tion due to inner stress caused by the rigidity of crosslinking during deformation which can be tuned with altering crosslinking density of the material.[14]

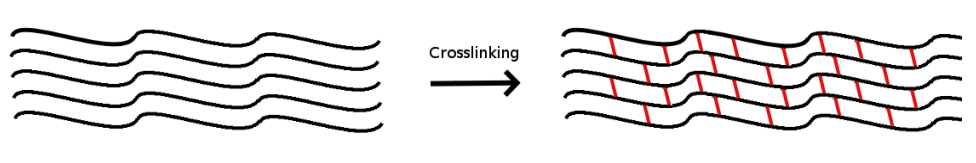


Figure 2.5 Crosslinking polymer chains. Covalent cross-links between the polymer chains, denoted here in red, connect two points of adjacent chains and thus improve material's reversibility of elastic stretching.

Consequently, liquid crystal elastomers (LCE) are polymers combining the elastic properties of an elastomer to the partial orientational order of LCs, resulting in a unique composite material with crosslinked polymer network's elastic properties with anisotropy. This combination opens abundant applications in photonics by having the optical properties of LCs on soft elastic matter. [15, 3]

2.3 Thermoactuated deformation

LCEs have proven to be a noteworthy topic of reasearch due in part to their ability to exhibit macroscopic deformation in the material through external stimuli, for example in photonics with photoactuated deformation. Combining controllable cooperative molecular motion with elasticity and sensitiveness of the soft elastomer materials, potential applications as photo-responsive actuators and microrobots are wide-ranging. These applications utilise thermal sensitivity of the material [16] or aptitude to light-induced *cis-trans*-isomerisation [17, 18] and thus macroscopic deformation together with controllable molecular alignment. These applications are discussed further in section 2.4.

2.3.1 Molecular alignment

Alignment of the LC molecules during polymerisation often determines the macroscopic response of the material to external stimuli. Hence controlling the molecular alignment is essential for applications relying on thermoactuated deformation. Effective methods for anchoring LC molecules to some preferred alignment involve electric fields or alignment layers. In the latter method, surfaces of substrates can be coated and treated with materials designed to guide the LC director in a desired direction.

Upon introducing LC molecules to the surface, the molecules realign along the director forming the desired molecular alignment. The aligned LCs can be polymerised with suitable crosslinkers and initiators to form a liquid crystal network (LCN), effectively perpetuating the alignment beyond the presence of an electric field or alignment layer. Creating a permanent LC alignment within LCE materials enables a myriad of photo- and thermoactuated applications discussed further in section 2.4.

For the purpose of this research, relevant molecular alignment types are *homeotropic*, *planar* and *splayed* alignments. LCE molecules aligned perpendicular to the material's surface are in homeotropic alignment, whereas molecular alignment parallel with the surface is known as planar. The combination of these two alignments where molecules on one surface are in planar alignment and on the other in homeotropic alignment is splayed nematic alignment. The materials used in this research were in splayed nematic alignment as illustrated in Fig. 2.6. For practical applications, the alignment of LCE molecules must be controlled on the surfaces of the material. The chemical methods of sample preparation to define the LCE molecule alignment is elaborated in more detail in section 3.1.

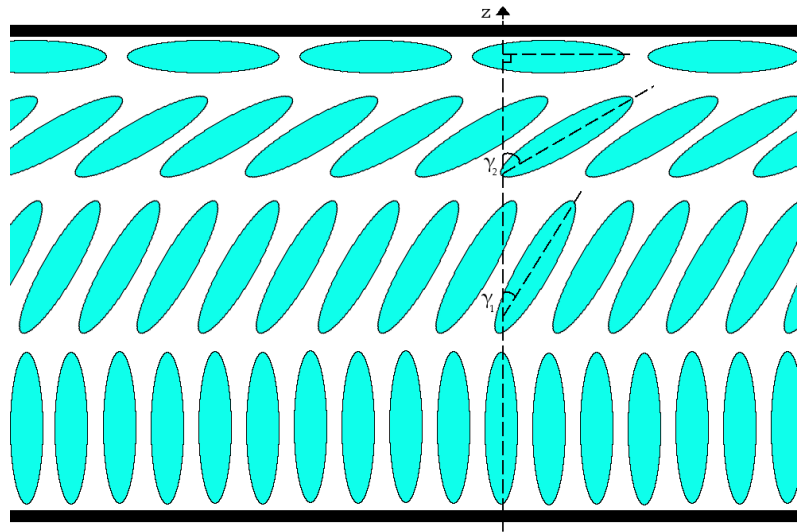


Figure 2.6 Splayed nematic alignment. One surface of the material (top) is polymerised in planar alignment, parallel with the surface, and the other (bottom) in homeotropic alignment, perpendicular to the surface.

Within the splayed nematic alignment, director of the molecules in the material near the homeotropic layer is in a small angle with the director of the homeotropic layer's director denoted in Fig. 2.6 as z-axis. Similarly, the molecules near the planar layer are aligned with a similarly small angle to the surface. These molecules therefore seek to align along the surface molecules' director creating a splayed alignment

within the material.

2.3.2 Thermal sensitivity

As discussed in section 2.1.1, the degree of orientational order denoted with the order parameter depends on the thermal motion of the molecules. Near the phase transition point T_c the LCE molecules demonstrate higher degree of orientational order than near the melting point T_m . With homeotropic alignment, the increased thermal motion of the molecules leads to expansion of the layer —the rod-like molecules are optimally packed with the director perpendicular to the surface, while thermal motion causes the average molecule to be with an angle to surface, causing the molecules to be packed less tightly. Contraction ensues with the planar alignment from increased thermal motion as molecules parallel to the surface become more tightly packed with an angle to the surface, respectively.

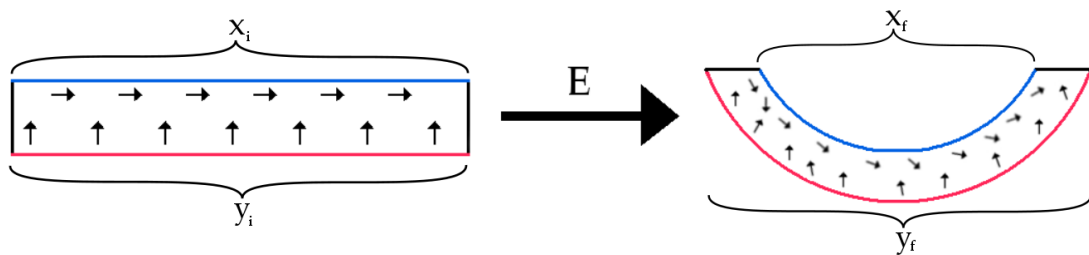


Figure 2.7 Thermoactuated deformation. Upon exposing the material to heat or irradiation, the thermal motion of the molecules increases and consequently the order parameter decreases, resulting in expansion on the homeotropic surface ($\Delta y > 0$) and contraction on the planar surface ($\Delta x < 0$) of the material.

With splayed nematic alignment, molecules on one surface of the elastomer are aligned in homeotropic layers while molecules on the other surface are in planar alignment. The aforementioned expansion and contraction thus occurs simultaneously in the material. This causes a macroscopic deformation illustrated in Fig. 2.7. Thermal motion can be induced by any means of transferring heat into the material, encouraging to photonics applications in particular as light absorbed by LCE is, in essence, energy converted into mechanical motion due to change in molecular alignment.[19]

Light- or heat-induced deformation can be observed in these external stimuli-deformed LCE systems, *actuators*, using remarkably low power on the material, indicating basis for cost-effective microrobotics.[19] Although photoactuators are intriguing research topics for their potential sunlight-powered applications alone, understanding

the process of thermoactuation and unraveling its potential for sensor applications is the motivation for this thesis. Photoactuators are equally sensitive to temperature changes and utilising the macroscopic deformation these temperature changes can be observed and measured.[20]

2.3.3 Adding some twist to it

The event of one-dimensional deformation of a splayed nematic LCE is illustrated in Fig. 2.7. When a strip of the material is cut along the planar director and heated up, the decreasing orientational order causes the macroscopic deformation. A similar deformation is observed when the strip is cut with an angle to the planar alignment director. However, increased thermal motion within the material deforms the strip along the director vector. Ensuing deformation is thus two-dimensional as illustrated in Fig. 2.8.

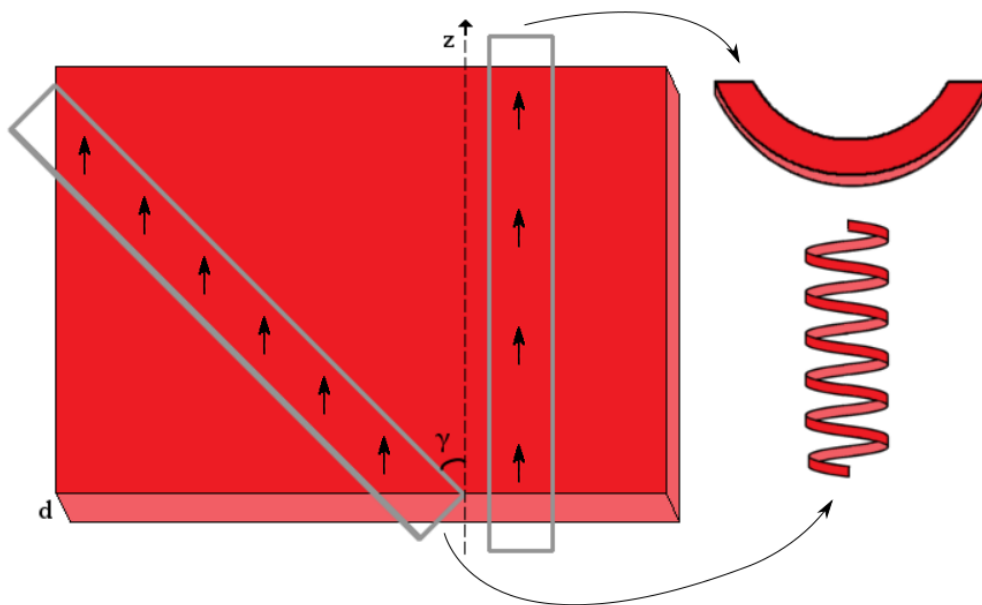


Figure 2.8 *Effect of planar alignment director angle to the deformation.* LCE strip cut from a sample of thickness d along its planar alignment layer's director z deforms one-dimensionally while LCE strip cut with an angle γ to the director results in two-dimensional deformation, a twist, resembling a coil. Arrows represent planar molecular alignment in the strip.

The elastic coil obtained by cutting the strip out with a $\gamma = 45^\circ$ angle yields a helical structure around its symmetry axis. [21] The *chirality* of the coil depends on the cutting: if the strip is cut out as depicted in Fig. 2.8, the coil is of left-handed

type, while cutting the strip out from the right-hand side of the material results in a right-handed type coil. [22] As with LCs in cholesteric phase, the pitch of the coil is defined as the longitudinal distance in which the coil has completed a full helix turn of 360° .

Given these premises, a hypothesis can be formulated: when fixed to a position from one end, heating the LCE coil leads to increased thermal motion within the material and hence deformation which can be observed by the twist of the tip of the coil. Correspondingly, cooling down the coil increases the degree of positional order within the material causing the coil to twist in the opposite direction. The motivation of this thesis work is to test the hypothesis and conceivably harness this phenomenon into a thermal sensor by characterising the angular twist of the coil as a function of temperature. The methods for testing the hypothesis as well as material characterisation are discussed further in chapter 3.

2.4 Applications

This section elaborates the wide range of versatile LC and LCE applications available to date. Liquid crystal displays (LCD) are perhaps the most widely known application of LCs. In essence, the optical properties of LCs alter in the presence of an electric field which enables display applications. [6] In an LCD, a thin LC layer is placed between two polarisers with perpendicular polarisation angles and often a reflective surface behind the aforementioned setup. The LC layer is aligned with an angle, typically 45° , with respect to the perpendicular polarisations. Propagating light interacts with the layer and reorients along its director, allowing some of the light to pass through the second polariser. If an electric field is applied to a part of the layer, however, the molecules in the area realign accordingly, resulting in a contrast between the field-affected area and the unaffected part of the layer preferable for a display.

While in twisted nematic alignment, the LC layer polarises light making the system partially transparent. Upon introducing an electric field into the layer, the molecules align parallel to the field, effectively revoking the polarising effect of the layer and rendering the system opaque. Controlling the optical properties with electric field with high precision enables extremely sharp image displays, and with color filtering the LCs form red, green and blue pixels (RGB) for vivid images. [6]

Incorporating LC molecules into elastomer chains have proven an ample source of innovative applications in the field of photonics. [20] The prospect of harnessing external source of stimulus such as light to power soft matter microrobotics and

perhaps ultimately converting sunlight into mechanical work in these actuators provides for a potent motivation to explore the possibilities of these actuators and the photomechanical actuation in particular. [19]

In recent years, one application for LCEs has been research on electronic artificial muscles. In these polymer-made muscles, LCEs generate mechanical work in the presence of an electric field. Although a promising application, the low modulus of elastomers together with the limited strain of the field-actuated molecules cannot currently compete with ferroelectric artificial muscle solutions in terms of work density. [23]

Other intriguing advances proposed in the field of light robotics are based on LCE strips used to mimic the motion of a caterpillar [24], iris [25, 26] and flytrap [27] by photoactuation. A simple splayed nematic alignment within the LCE results in a single-direction bending due to release of inner stress upon removing a strip. Given a sample with stripes of alternating splayed nematic alignment, however, results in a strip bent from multiple points in a meandering fashion. In a strip with such alignment stripes, a caterpillar, one stripe has homeotropic and planar alignment layers on opposite sides of the material as the next stripe. This type of alignment leads to a snake-like curvy shape enabling caterpillar locomotion. [24]

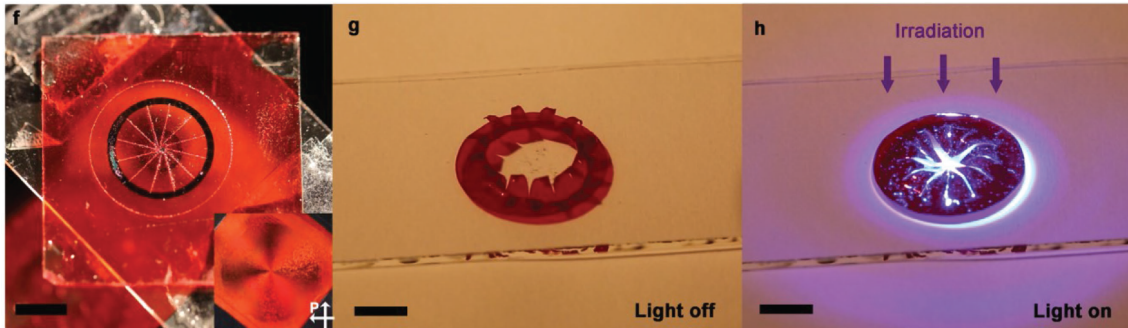


Figure 2.9 Schematic of the LCE iris. (f) Cutting the iris out of the sample with 12 pedal-like segments. (g) Soft LCE iris in its relaxed state without illumination and (h) the iris closes upon illumination. [26]

Similar photoactuation can be observed with a LCE iris. Utilising *photoalignment* [19, 26] to manufacture a spherical splayed nematic alignment and dissecting twelve symmetrical segments from the centre of the circle produces a light-controllable iris-like shape as shown in Fig. 2.9. The initial bending of the segments can be engineered by adjusting the sample preparation conditions, leaving the orifice of the iris initially open if desired. Upon illumination the aligned molecules within the segments heat up and cause a reduction to the orientational order and thus deformation, effectively closing the iris.

While the iris actuator allows for light-sensitive regulation of an orifice, LCE-based artificial flytrap grips objects based on reflection. An optical fiber is attached to a transparent hole in the middle of the LCE strip perpendicular to the LCE surface. A beam of light propagates equally perpendicular from the surface with nominal absorption to the LCE thus causing no deformation as illustrated in Fig. 2.10 c. When an object intercepts the beam of light, however, a considerable amount of light is reflected from the object to the elastomer. The absorbed light causes deformation in the LCE towards the object. Due to the bending, more LCE surface is exposed to reflected light and thereby bent towards the object resulting in a gripping motion.

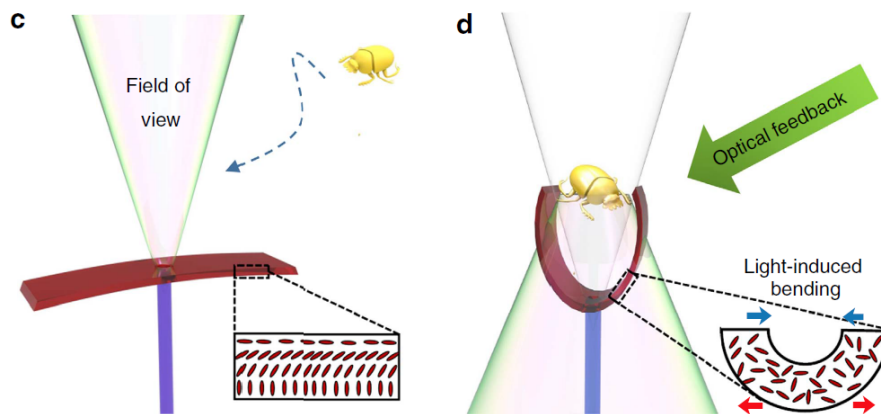


Figure 2.10 Flytrap-inspired light-powered soft robot. (c) Beam of light propagating from the optical fiber is not absorbed into the material until an object blocks the beam and reflects the light onto the elastomer. (d) Light reflecting from the object causes grip-like bending in the elastomer, effectively capturing the object.[27]

Given the thrilling nature of LCE materials and their immense potential for photonics applications, it is safe to assume the research on light-fueled soft material microrobotics is yet to unravel countless inspiring ways to develop new uses and materials in the field of polymeric actuators.

3. SAMPLE PREPARATION AND METHODS

In order to characterise the thermal sensitivity of the LCE strip, a sample of desired thickness was prepared and a suitable experimental setup devised. This chapter delves into sample preparation, experimental setup for the measurements and data processing methods for the measurement results.

3.1 Preparing the sample

The LCE was prepared from a mixture containing:

- LC monomer 4-Methoxybenzoic acid 4-(6-acryloyloxyhexyloxy)-phenyl ester,
- LC crosslinker 1,4-Bis-[4-(3-acryloyloxypropyloxy)- benzoyloxy]-2-methylbenzene,
- light-responsive molecule N-Ethyl-N-(2-hydroxyethyl)-4-(4-nitrophenylazo)-aniline, and
- less than 1 % molar proportion of photo-initiator 2,2-Dimethoxy-2-phenylacetophenone.

The structural formulas of the components relevant for this thesis in the monomer mixture are shown in Fig. 3.1. LC monomer provided the material with properties characteristic to liquid crystals while crosslinker brought rigidity. A photoisomerisable dye often used in devising photoactuators was added to soften the material. The mixture was prepared in the presence of a solvent to ensure homogeneous mixing.

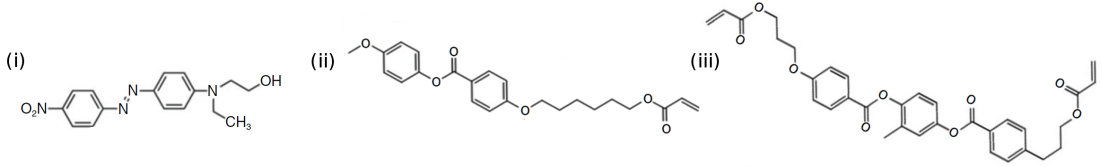


Figure 3.1 Molecules and their mole fraction in the monomer mixture. (i) 2 mol% Disperse Red 1 photoisomerisable dye, (ii) 77 mol% LC monomer and (iii) 20 mol% LC crosslinker.

In order to align the molecules in the mixture during polymerisation, two glass substrates were *spin coated*, one with polyvinyl alcohol (PVA) and another with polyimide (PI) alignment layers by applying a drop of dilute aqueous solution on the center of the glass coverslip and rotating the substrate. The centrifugal force spreads the material uniformly on the substrate and simultaneously expels excess fluid off the edges of the flat surface. Due to the volatility of the fluid, the coating film reaches an equilibrium thickness determined by the angular speed of the rotation and the concentration of the solution. [28]

PVA and PI films function as alignment layers for the LCE molecules on the glass substrate. PI surfactants induce *homeotropic* alignment in the LCE molecules, causing the rod-like molecules to align perpendicularly to the surface. [20] PVA film was then unidirectionally rubbed with a satin cloth to produce microgrooves on the polymer surface along which the LCE molecules can align, parallel to the substrate.[9]

Both substrates were then cleaned with compressed nitrogen gas to remove any unwanted particles prior to LCE polymerisation. The microscope slides were subsequently attached together with alignment layers facing each other to form a cell to produce the LCE of specific thickness. To determine the thickness, microscopic inert spacers of diameter $d = 20 \mu\text{m}$ were placed to the opposing corners of the substrates with UV glue. LED light was used to cure the glue thus solidifying the cell.

The LCE monomers were then heated to 70 °C, magnetically stirred into a homogeneous mixture and injected into the cell at 70 °C with capillarity due to the 20 μm space between the glass substrates. Upon cooling the mixture down to 30 °C, the monomer molecules on the interface of alignment layers orientated along the layers' director vectors \vec{n}_i forming a splayed nematic alignment which was photopolymerised with 385 nm UV light. LCE strips suitable for the measurements were subsequently cut from the sample and attached onto a glass substrate with UV glue and a piece of optic fibre to ensure the longitudinal shape of the LCE coil.

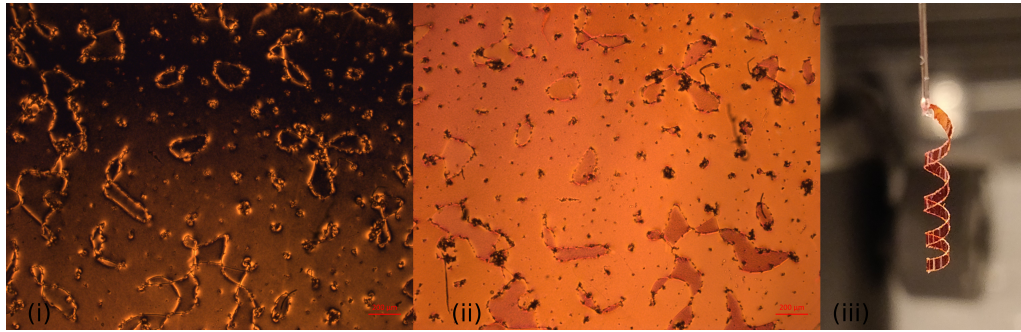


Figure 3.2 Images of the LCE material. (i) A polarised microscope image of the LCE with the domain's director in parallel with one of the polarisers, (ii) same material with the stage rotated an angle of $\theta = 45^\circ$ and (iii) a picture of the LCE coil attached to an optic fiber.

Images taken from the strips cut from the sample are presented in Fig. 3.2. The same phenomenon is observed in the first two images, (i) and (ii), as in Fig. 2.3. At first, the director of the monodomain material is in parallel with one of the polarisers in the microscope setup, resulting in less light to the camera. Correspondingly, upon rotating the microscope stage 45° more light is detected by the camera due to light's interaction with the material which modulates the polarisation of the light. Therefore less light is polarised perpendicular to the analyser and the second image is brighter than the first. The third image is taken from a LCE strip attached to the optical fiber for potential thermal sensing applications.

3.2 Experimental setup

To determine the thermal sensitivity of the LCE strip, an experimental setup for the measurement was devised as shown in Fig. 3.3. The coiled LCE strip was stationed to hang freely from the top of qpod 2e [29], a customisable temperature-controlled sample compartment. The compartment was filled with air and kept thermally stable but not hermetic. The glass substrate carried the weight of the coil so the force of gravity stretched it perpendicular to the substrate and consequently to the surface of the table.

Inside the qpod, a mirror surface was placed in a 45° angle with respect to table surface. A source of white light was positioned above the qpod in order to illuminate the coil. The light reflected from the mirror surface and subsequently through a hole on the qpod's side as shown in Fig. 3.3 (ii). Reflected light was detected by Canon EOS 5D Mark III system camera.

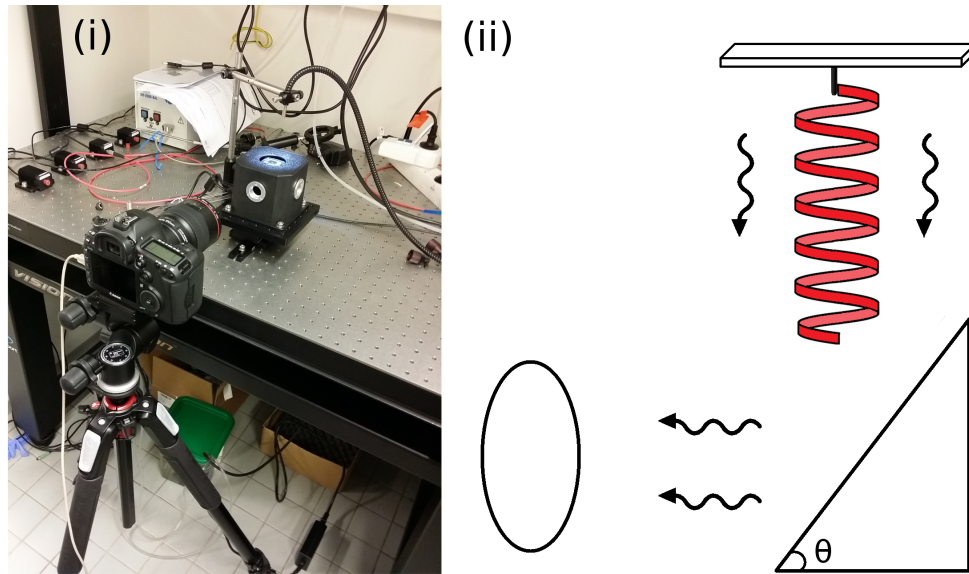


Figure 3.3 Experimental setup. (i) Devices used in the measurement and (ii) a diagram of the measurement, $\theta = 45^\circ$.

The temperature within qpod's compartment could be thermally controlled with high precision within the temperature range of the LCE's nematic phase and thus was chosen for controlling the temperature of the LCE coil. Upon heating, the homeotropic alignment layer in the LCE strip expands due to thermally induced alignment change, while the layer aligned in the direction of the rubbing contracts, respectively. This causes the coil to 'uncoil' and simultaneously lengthen towards the mirror surface by twisting the coil's tip following a helical path in clockwise motion as shown in Fig. 3.4.

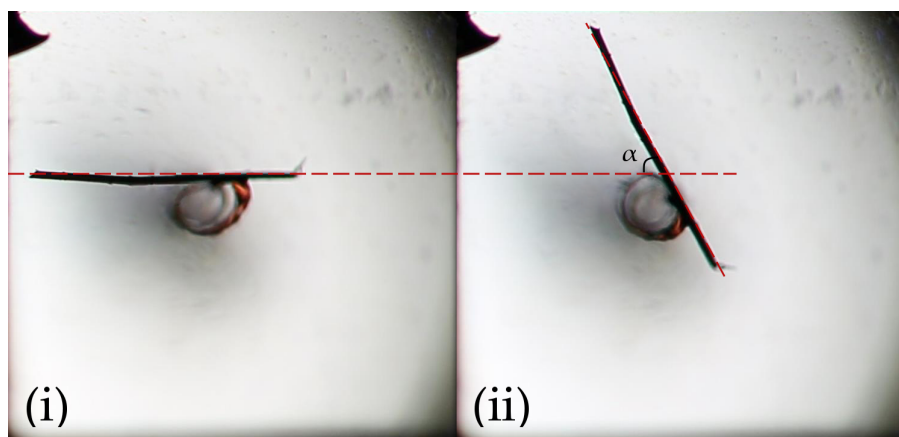


Figure 3.4 Clockwise motion of the coil's tip. The piece of hair attached to the coil's tip turns like a hand on a clock between temperatures $T_i = 20,00^\circ\text{C}$ and $T_{ii} = 23,12^\circ\text{C}$. Angular change $\alpha = 62,3^\circ$.

Consistently, cooling down the compartment and the coil within results in counterclockwise motion of the tip on a helical path towards the glass substrate, i.e. contraction and 'coiling' of the LCE strip. This deformation of the strip can be characterised by the angular change of the tip of the coil as a function of temperature. By taking a series of images of the view reflected from below the coil and measuring the temperature of the coil, the angular change per Kelvin can be determined and hence the sensitivity of the sensor.

3.2.1 Determining the relaxation time

During preliminary experimentation with the measurement setup, a question was raised: at a given temperature, how long will the LCE strip continue to deform? It was observed that the coil evidenced prolonged deformation at a thermally stable condition for an extended period of time. The first measurement, therefore, was to measure the time required for the deformation of the coil to saturate and thus define the relaxation time τ for the LCE strip, i.e. the amount of time required for the inner stress of the material caused by the thermal expansion and contraction of opposite surfaces of the film to be released.

Once the relaxation time τ was defined, the reproducibility could be determined by measuring the eventual angle of the tip of the coil in given temperatures after similar temperature change. The length of the reproducibility measurement would greatly depend on the relaxation time of the material.

3.2.2 Measuring the sensitivity

The sensitivity of the sensor depends on the thermally induced angular change of the coil's tip as the greatest resolution achievable is determined by the minimum variation in temperature dT to produce detectable angular change in the coil. The thermistor built into the qpod 2e is limited to thermal resolution of $\Delta T \approx 0,01^\circ\text{C}$ so to measure the sensitivity of the coil it is prudent to measure its angular change with respect to $0,01^\circ\text{C}$ which corresponds to the precision of the measurement. Height of the qpod limits the measurement range, however, as does the nematic phase temperature range of the LCE.

Furthermore, the angular change as a function of temperature was measured with several thermal gradients to determine the effect of rapidity of temperature change to the angular change of the coil's twist. To minimise the effect of random errors, both types of measurements were taken with numerous repetitions.

3.3 Processing the data

Aforementioned measurements will accumulate a considerable amount of images and data on the qpod's compartment's temperature. Due to the thermally stable nature of the compartment and the low heat capacity of air, its temperature is henceforth considered analogous to that of the coil. The angular change of the coil is analysed from the recorded images using ImageJ processing software and in particular its TrackMate plugin. The angular data is then paired with corresponding thermal data and processed using MATLAB.

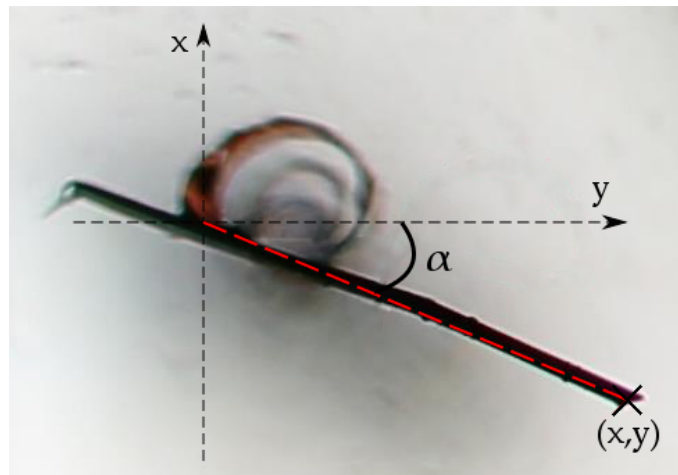


Figure 3.5 Computing the angle of the twist. A normalised vector based on the coordinates of the tip of the coil and the tip of the hair was used to compute the angle of the twist.

As depicted in Fig. 3.5, each recorded image was cropped with ImageJ and within the images, coordinates of the end of the LCE coil as origo and the tip of the hair (x, y) were computed. With the position vector of the tip of the hair, the angle of the twist was calculated with respect to the positive y-axis as shown in Fig. 3.5. These angles were then combined with the corresponding temperature values from the qpod in-built sensor data. Using a normalised position vector \vec{v} for the tip of the hair, the angle of the twist is

$$\alpha = \arctan\left(\frac{y}{x \cdot \sqrt{x^2 + y^2}}\right). \quad (3.1)$$

where the term $\sqrt{x^2 + y^2}$ is the length of the vector \vec{v} .

4. RESULTS AND DISCUSSION

A total of 15 measurements were conducted to determine the sensitivity of the temperature sensor and the reproducibility of the experiments. This chapter presents the data from the measurements and discussion on the results.

To improve the resolution of the measurement, a piece of hair was UV-glued to the tip of the LCE strip to function as a hand on a clock. The mass of the hair was insignificant compared to the elastomer and was thus approximated to be massless. Even if the hair is not perpendicular to the vertical axis of the coil but tilted towards the mirror surface, the measured angle of the coil remains the same.

4.1 Relaxation time

The first measurement was conducted to determine the reproducibility of the experiments. The LCE strip was heated from $T_i = 20^\circ\text{C}$ to $T_f = 30^\circ\text{C}$ within a two-second timeframe. The angular change was then monitored and recorded with the camera setup. For the first minutes of the measurement, images of the twist were recorded with 5 second intervals. Once the rapid twisting of the coil had ceased, the interval of imaging was changed to 1 min.

Measured angles with respect to time are visualised in Fig. 4.1 as blue dots. The measurement was carried out for 212 minutes, although the rapid twisting of the coil ended at 6 min marker and prominent saturation was detected at $t = 150$ min. Maximum angle of twist reached during the measurement was $\theta_{max} \approx 535^\circ$. Despite being kept at constant temperature for over three and a half hours, the coil persisted to twist, albeit after 150 minutes the angular change of the twist was extremely slow: during the last hour of the measurement, the measured angular change was $\Delta\theta_{150 \text{ min} \rightarrow 212 \text{ min}} = 6,4^\circ$ or 1,2% of the overall angular change.

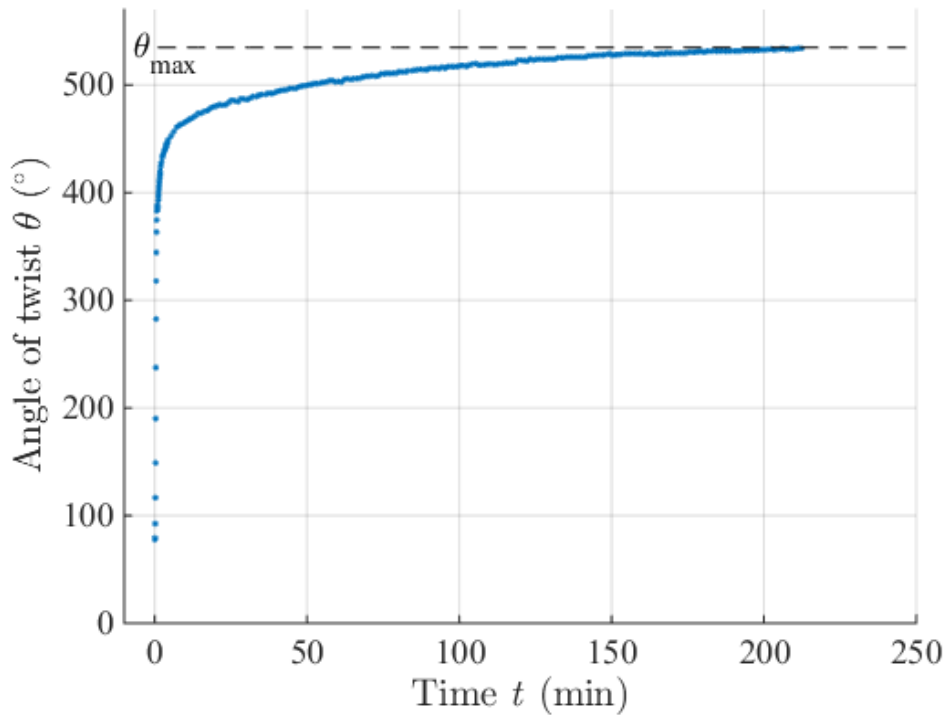


Figure 4.1 Relaxation time of the LCE strip. Actuated by a rapid temperature change from 20°C to 30°C , the ensuing twist in the LCE coil was recorded. Maximal measured twist $\theta_{max} = 535^{\circ}$.

From Fig. 4.1, three distinct stages can be observed. First, the stage of rapid angular change takes place during the first minutes of the measurement. Followed by over two hours of constantly decreasing angular acceleration, the second stage consists of gradually diminishing inner stress caused by increased thermal motion. Lastly, in the third stage the angular acceleration has saturated and the change in the angle of twist is minimal. The relaxation time of the coil is therefore estimated to be $\tau \approx 150$ min.

Motivated by the results, another measurement for reproducibility was conducted. The LCE coil was kept at 20°C temperature for 150 minutes, after which it was quickly heated to 30°C and kept at constant temperature for another 150 minutes. The process was then repeated by quickly cooling down to 20°C temperature for 150 minutes and subsequently heating the coil up to 30°C temperature for 150 minutes. The angle of the coil was measured at four points of time just before altering the qpod compartment temperature. The goal was to determine whether the coil would reach the same angle of twist twice in time τ given identical temperature gradient. Measured angles are presented in table 4.1.

Table 4.1 Determining reproducibility of the measurements. Measured angles were normalised with respect to starting angle at $t = 150$ min.

Time, temperature	Angle
150 min, 20 °C	0,0°
300 min, 30 °C	530,2°
450 min, 20 °C	12,6°
600 min, 30 °C	517,4°

The corresponding angles were not identical. A deviation of approximately 13° was observed in both temperatures after equal relaxation time. Compared to the total angle of twist, however, the deviation is considerably small, under 3%, so the measurement can be considered repeatable within this magnitude of error.

The deviation is most likely caused by random error with the measurement due to non-uniform flow of heat from the Peltier device through the air medium to the LCE coil. Imperfect sample preparation conditions may leave impurities within the material affecting the measurement, and the measurement compartment within the qpod was not entirely air-tight. Given these circumstances, the deviation between the measured angles is within the limits of error.

4.2 Measurements of angular change

Angular twist of the LCE coil was then measured in the temperature range of 20 °C to 30 °C with temperature gradients of three magnitudes. First, the material was heated from 20 °C to 30 °C at a rate of 2 °C/min and subsequently cooled down to 20 °C at the same rate. Angle of the coil's tip was observed and imaged with 5 s time intervals. The measured angles of the first measurement are shown as a function of temperature in Fig. 4.2.

The LCE coil was first heated for five minutes from 20 °C to 30 °C with a temperature gradient of 2 °C/min and subsequently cooled down back to 20 °C at an equal rate. First results denoted by blue dots were measured in a measurement compartment without semi-air-tight conditions, i.e. without blocking the flow of hot air from the compartment. As evident in Fig. 4.2, the results clearly diverge from the other measurements during and after approaching the 30 °C threshold, potentially due to the flow of air within the measurement compartment.

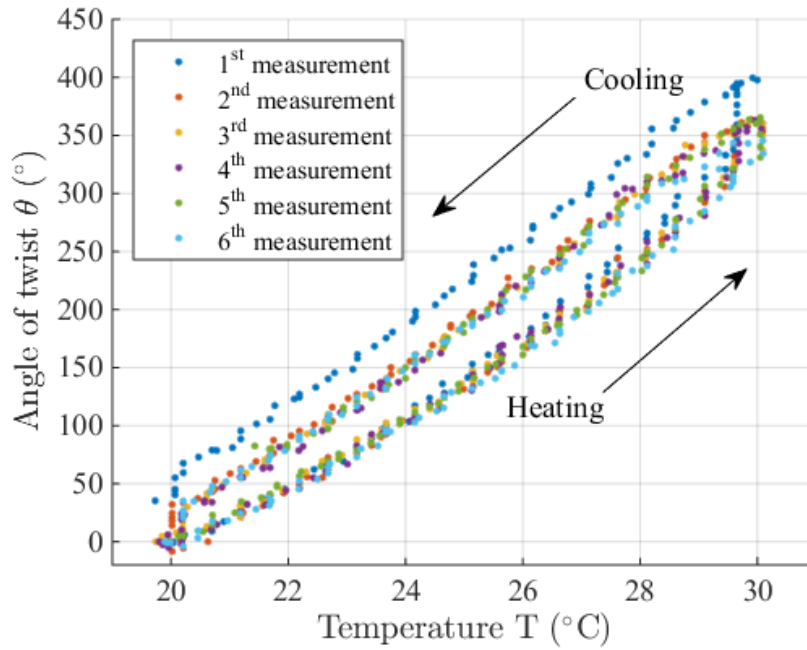


Figure 4.2 Measured angle for $2\text{ }^{\circ}\text{C}/\text{min}$ rate.

After improving the measurement setup by blocking the flow of hot air from the compartment with transparent glass substrates, the other five measurements were carried out on different days over a period of several weeks. The results, however, correspond to each other with little deviation: the mean angular deviation of each measurement from their average is presented along with the maximum angle of twist in table 4.2. The first measurement was excluded from computing the mean values of the measurement due to different experimental conditions.

Table 4.2 Mean deviation of first measurements from the average values.

*1st measurement was excluded while calculating average values.

Measurement	Angular deviation $\Delta\theta$	% from max value	Maximum angle $\theta_{1,max}$
1 st	28,1°	7,02%	399,5°
2 nd	10,9°	3,00%	363,6°
3 rd	10,1°	2,81%	361,0°
4 th	8,76°	2,41%	363,0°
5 th	10,6°	2,90%	365,4°
6 th	4,92°	1,42%	345,6°
Average*	8,57°	2,38%	359,7°

As seen in the data presented in table 4.2, the average maximum angle of twist

for ten degree temperature change is $\theta_{1,max} \approx 360^\circ$ or one full twist of the LCE coil. The angle of the twist is considerably smaller than the maximal angle in the relaxation time measurement. Corresponding angle occurred in the relaxation time measurement after 40 seconds of the measurement. The temperature gradient of the relaxation time measurement was orders of magnitude greater than in the six measurements with $2^\circ\text{C}/\text{min}$ heating rate, however, so the results are not directly comparable.

Computing mean values from the data accurately represents the measurements as shown by low percentage of deviation of 2,38%, a deviation within the magnitude of error from the measurement of reproducibility. Based on these results, approximately $36^\circ/\text{K}$ angle of twist would be observed in a thermal LCE sensor with a temperature gradient of $2^\circ\text{C}/\text{min}$, while the sensitivity of the LCE was commendable – first noticeable angular change was observed after $0,1^\circ\text{C}$ degree change.

Similar angular change was observed when the material was correspondingly heated and cooled with the rate of $1^\circ\text{C}/\text{min}$. Angles of the coil's tip are presented in Fig. 4.3. Moreover, a similar deviation in the first measurement is observed due to identically different experimental conditions as with the first set of measurements. Although the temperature gradient was half of that in the previous measurements and the measurement thus twice slower, a similar deviation persists.

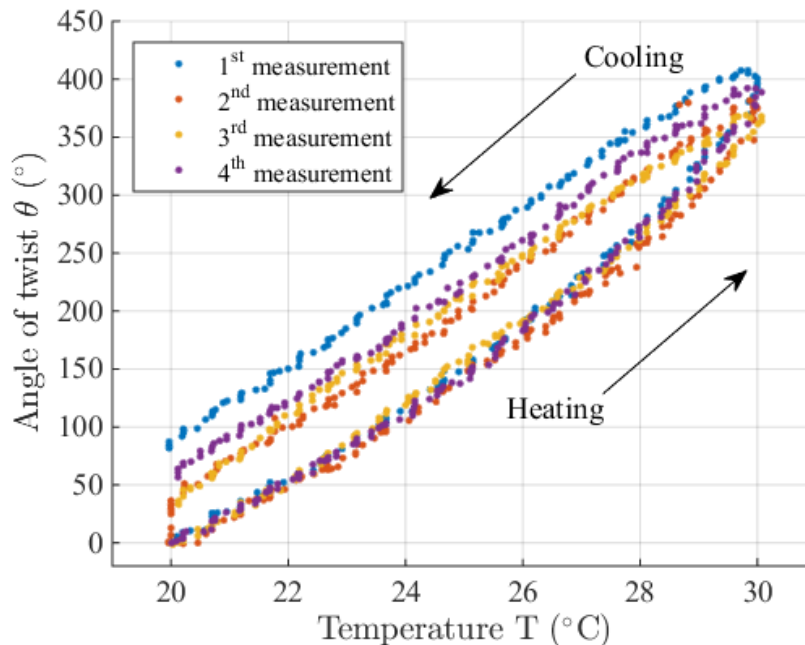


Figure 4.3 Angular change for the $1^\circ\text{C}/\text{min}$ measurement.

The three other measurements with a temperature gradient of 1 °C/min followed a similar trend as with the first set of measurements by being relatively coincident. It is noteworthy, however, that the angular change difference between the measurements is more prominent during the cooling down from 30 °C to 20 °C than prior to reaching the 30 °C threshold. Maximum angles of twist as well as angular deviations between the second set of measurements are presented in table 4.3. The increased deviation in the angle of twist is evident when comparing the mean deviations of the first and second set of measurements: with a temperature gradient of 1 °C/min, the average percentage of deviation exceeds the magnitude of error from the measurement of reproducibility. Furthermore, the average maximum angle from the measurement is 5,9% greater than with the lower temperature gradient or approximately 38°/K. This indicated the rate of temperature change has an impact on the maximum angle observed as to the reproducibility of the measurement. Similar sensitivity was observed as before: first noticeable twist occurred at 20,1 °C. The maximum angle of the twist was correspondingly smaller than the maximal angle in the relaxation time measurement with a similar angle occurring at $t = 63$ s while measuring τ .

Table 4.3 Mean deviation of second measurements from the average values.
**1st measurement was excluded while calculating average values.*

Measurement	Angular deviation $\Delta\theta$	% from max value	Maximum angle $\theta_{2,max}$
1 st	27,9°	6,86%	407,5°
2 nd	13,6°	3,57%	381,6°
3 rd	14,2°	3,85%	368,9°
4 th	17,8°	4,54%	392,3°
Average*	15,2°	3,99%	380,9°

Providing the long relaxation time of LCE used in these measurements, it is conceivable for the coil to twist into a greater angle given a lower temperature gradient and thus more time to twist within the same temperature range. To further determine the effect of the temperature gradient on the angle of twist, a third set of measurements were taken with a temperature gradient of 0,5 °C/min. The results of the measurement are represented in Fig. 4.4. As can be seen from the figure, the angular deviation between measurements is even slightly greater than with the 1 °C/min measurement. In addition, the second measurement produced an unexpectedly high peak angle at the temperature of 30 °C threshold. This peak could be a result of a measurement error but is still included in the average results calculation due to its otherwise coherent shape of data.

As seen in Fig. 4.4, the mean maximum angle of the third set of measurements

was even higher than with that of the second set of measurements. This supports the notion of temperature gradient affecting the maximum angle due to the long relaxation time of the LCE. Another observation similar to the second measurements can be made: heating up the coil resulted in nearly identical angular change with respect to temperature, while the cooling down resulted in differing outcomes despite seemingly similar experimental conditions. This suggests that a sensor application with LCE materials would yield more reliable readings with a positive temperature gradient rather than negative.

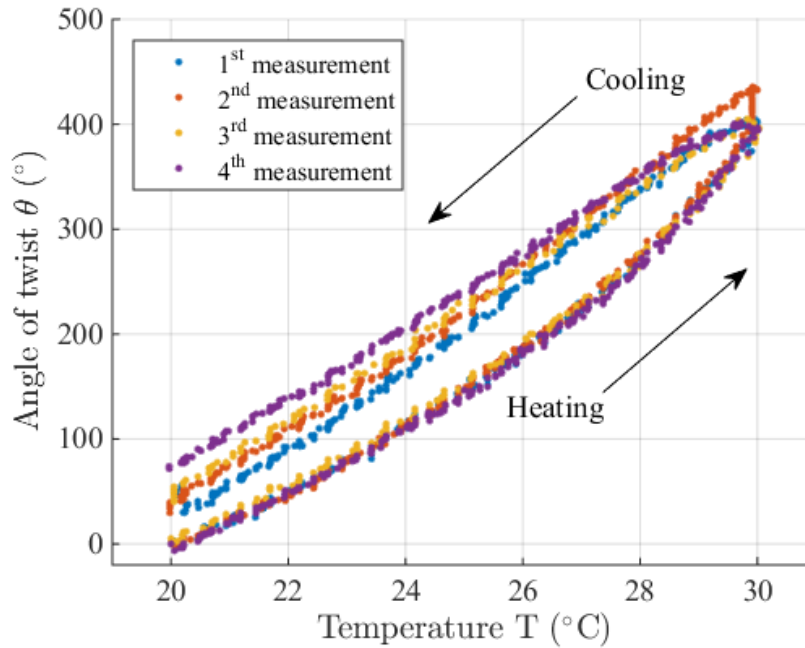


Figure 4.4 Angular change for the 0,5 °C/min measurement.

To determine the effect of the lowest temperature gradient, maximum angles of twist as well as angular deviations between the third set of measurements were calculated. These values are presented in table 4.4. As evident from Fig. 4.4, angular deviation between measurements is even greater than with the second set of measurements with an average angular change of 40 °/K. Although the maximum angle is still over 20% smaller than the angles measured with relaxation time, where the corresponding angle occurred at $t = 90$ s, the maximum angle $\theta_{3,max}$ is 5,9% greater than $\theta_{2,max}$. This would suggest an inverse relation between the temperature gradient and the maximum angle of twist in the LCE coil. Based on these results, outline of the relation between the temperature gradient and the maximum angle of the twist can be formulated to be

$$\frac{G}{n} \propto 1,059^n \theta_{max}, \quad (4.1)$$

where G is the temperature gradient, θ_{max} is the maximum angle of the twist and n is a scalar factor. With regard to sensor application, the inverse relation between the temperature gradient and the maximum angle of twist indicates higher thermal resolution but lower reproducibility with lower temperature gradient, i.e. slower rate of temperature change.

Table 4.4 Mean deviation of third measurements from the average values.

**Peak of the 1st measurement was excluded while calculating average values.*

Measurement	Angular deviation $\Delta\theta$	% from max value	Maximum angle $\theta_{3,max}$
1 st	22,0°	5,45%	404,5°
2 nd	25,6°	5,88%	435,4°
3 rd	11,6°	2,86%	404,9°
4 th	22,9°	5,70%	401,5°
Average*	20,5°	5,09%	403,6°

As shown in table 4.4, the angular deviation between the measurements was almost twice the deviation in the measurement with relaxation time $\tau = 150$ min. However, the average shape of the data in Fig. 4.4 is still coherent with the measured phenomenon.

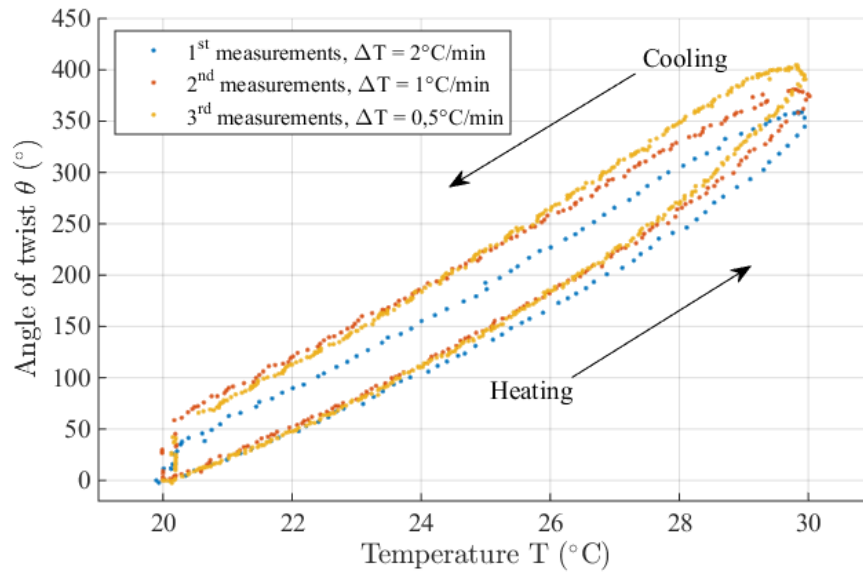


Figure 4.5 Mean angles of twist as a function of temperature for the measurements.

Given the increased maximum angle in each consecutive measurements with different temperature gradients, the averaged results from the three sets of measurements align to some extent when plotted as a function of time. These averaged values of the angles of twist are presented in Fig. 4.5 with maximum angles as peaks of the data points. Similarly, the measured angles of twist diverge from each other marginally between temperatures 20 °C and 24 °C, while the angular deviation is greatest near the 30 °C threshold. In all three sets of measurements, first distinct twist occurred after 0,1 °C temperature change.

The relation expressed by equation 4.1 seems to contradict the measured maximum angles of the relaxation time measurement. However, the relaxation time measurements were conducted with a temperature gradient two orders of magnitude greater than the measurements of angular change. Therefore the comparison between the results of the phenomena is complicated but nontrivial. The equation 4.1 is a valid reference point for the inverse relation between the temperature gradient and the maximum angle of the twist within a certain range of gradients. Notwithstanding, further research on the topic of gradient-dependence of the maximum angle is needed.

5. CONCLUSIONS

To determine the suitability of LCE strip for thermal sensor applications, an experimental setup to measure its thermal sensitivity was devised. After extensive research on LCs and LCEs, a sample was prepared and a strip cut from it with a 45° angle with the planar alignment layer's director to ensure a helical shape. The helical LCE strip, a coil, was fixed from one point to hang freely in a thermally stable measurement compartment above a mirror surface with which the coil could be observed from below. The measurement compartment and consequently the coil was then periodically heated and cooled while observing the angular change in the freely hanging tip of the coil through means of a system camera. Angular data of the LCE was subsequently recorded and combined with temperature data from the measurement compartment's thermal sensor prior to computational analysis.

Through data analysis a high thermal sensitivity in the LCE strip was reported: the coil demonstrated visible macroscopic deformation, a twist, after 0,1 °C temperature change as well as a long relaxation time of $\tau = 150$ min. Furthermore, a considerable reproducibility was recorded with an average deviation of 2,4—5,1 % of angular deviation between the measurements and averaged data points. Three sets of measurements were carried out to determine the impact of temperature gradient on the sensor's performance. An inverse relation between the temperature gradient and the maximum angle of twist was observed as formulated in equation 4.1. In addition, an increase in the angular deviation of the measurements was discovered upon reducing the temperature gradient, suggesting lower reproducibility with slower measurements which is in accordance with the long relaxation time of the LCE.

The results of this research show great promise in a LCE-based thermal sensor. Given the soft and thus easily modifiable structure as well as the high thermal resolution that the measured sensitivity of the strip, LCE materials can provide competitive alternatives to modern thermal sensors with theoretical operating temperatures from below room temperature up to 200 °C. [26] Although the height of the compartment as well as the size of the LCE coil limited the measurable temperature range, the measurements were easy to conduct with good repeatability.

The LCE coil used in this thesis work reached thermal resolution of 0,1 °C which is the resolution of an average LC thermometer. [30] Improving the elastic properties of material by reducing crosslinking and film thickness while increasing the concentration of photoisomerisable dye would yield greater thermal sensitivity and thus enhanced resolution, for example. Furthermore, reducing the thickness of the hair indicating the angular change would increase resolution of the measurement considerably. Similar effect can be achieved by lengthening the coil as equal thermal change to a longer coil results in larger angular change. Combining the aforementioned improvements it is plausible to reach at least an order of magnitude greater thermal resolution.

A more detailed characterisation of the material is needed for a practical sensor application, however. Interesting topics for further research include determining the effective measurable temperature range, characterising the angular changes and maximum angles with several temperature gradients and exploring the optimal thermal resolution of the sensor. An equally interesting question arose during the measurements: why is the maximum angle of the relaxation time measurement considerably greater than those with orders of magnitude smaller temperature gradient? A study regarding very high and low temperature gradients would be particularly interesting.

REFERENCES

- [1] P.J. Collings. *Liquid Crystals: Nature's Delicate Phase of Matter*. Princeton University Press, 2002.
- [2] G. R. Luckhurst. Orientational order in liquid crystals: Experiment and theory. *Berichte der Bunsengesellschaft für physikalische Chemie*, 97(10):1169–1187, 1993.
- [3] Hao Zeng. *Light Driven Microscopic Robot (PhD thesis)*. PhD thesis, LENS - European Laboratory for Non-Linear Spectroscopy / University of Florence, 2015.
- [4] I.C. Khoo and S.T. Wu. *Optics and Nonlinear Optics of Liquid Crystals*. Series in Nonlinear Optics. 1993.
- [5] V.G. Chigrinov. *Liquid Crystal Devices: Physics and Applications*. Artech House optoelectronics library. Artech House, 1999.
- [6] Christopher Booth and Peter Raynes. Liquid – crystal displays. *Physics World*, 10(6):33, 1997.
- [7] A.A. Sonin. *The Surface Physics of Liquid Crystals*. Gordon and Breach Publishers, 1995.
- [8] M. Warner and E.M. Terentjev. *Liquid Crystal Elastomers*. International Series of Monographs on Physics. OUP Oxford, 2003.
- [9] Danish Iqbal and Muhammad Haris Samiullah. Photo-responsive shape-memory and shape-changing liquid-crystal polymer networks. *Materials*, 6(1):116–142, 2013.
- [10] Christian Bahr. *Smectic Liquid Crystals: Ferroelectric Properties and Electroclinic Effect*. Chirality in Liquid Crystals. Springer New York, 2001.
- [11] Morris S. Coles, H. Liquid-crystal lasers. *Nature Photon*, 4:676–685, 2010.
- [12] Tomiki Ikeda, Jun-ichi Mamiya, and Yanlei Yu. Photomechanics of liquid-crystalline elastomers and other polymers. *Angewandte Chemie International Edition*, 46(4):506–528, 2007.
- [13] Marc Soto, Rosa María Sebastián, and Jordi Marquet. Photochemical activation of extremely weak nucleophiles: Highly fluorinated urethanes and

- polyurethanes from polyfluoro alcohols. *The Journal of Organic Chemistry*, 79(11):5019–5027, 2014. PMID: 24820955.
- [14] A.A Askadskii. Influence of crosslinking density on the properties of polymer networks. *Polymer Science U.S.S.R.*, 32(10):2061 – 2069, 1990.
- [15] Kenji Urayama. Selected issues in liquid crystal elastomers and gels. *Macromolecules*, 40(7):2277–2288, 2007.
- [16] Taylor H. Ware, Michael E. McConney, Jeong Jae Wie, Vincent P. Tondiglia, and Timothy J. White. Voxelated liquid crystal elastomers. *Science*, 347(6225):982–984, 2015.
- [17] Zahid Mahimwalla, Kevin G Yager, Jun-ichi Mamiya, Atsushi Shishido, Arri Priimagi, and Christopher J Barrett. Azobenzene photomechanics: prospects and potential applications. *Polymer Bulletin*, 69(8):967–1006, 2012.
- [18] Arri Priimägi. Polymer-azobenzene complexes: from supramolecular concepts to efficient photoresponsive polymers, 2009.
- [19] Arri Priimagi, Christopher J Barrett, and Atsushi Shishido. Recent twists in photoactuation and photoalignment control. *Journal of Materials Chemistry C*, 2(35):7155–7162, 2014.
- [20] Christian Ohm, Martin Brehmer, and Rudolf Zentel. Liquid crystalline elastomers as actuators and sensors. *Advanced Materials*, 22(31):3366–3387, 2010.
- [21] Supitchaya Iamsaard, Sarah J. Akhoff, Benjamin Matt, Tibor Kudernac, CornelissenJeroen J. L. M., Stephen P. Fletcher, and Nathalie Katsonis. Conversion of light into macroscopic helical motion. *Nat Chem*, 6(3):229–235, Mar 2014. Article.
- [22] Kenneth D. Harris, Ruud Cuypers, Patrick Scheibe, Casper L. van Oosten, Cees W. M. Bastiaansen, Johan Lub, and Dirk J. Broer. Large amplitude light-induced motion in high elastic modulus polymer actuators. *J. Mater. Chem.*, 15:5043–5048, 2005.
- [23] Tissaphern Mirfakhrai, John D.W. Madden, and Ray H. Baughman. Polymer artificial muscles. *Materials Today*, 10(4):30 – 38, 2007.
- [24] Hao Zeng, Owies M Wani, Piotr Wasylczyk, and Arri Priimagi. Light-driven, caterpillar-inspired miniature inching robot. *Macromolecular Rapid Communications*, 2017.

- [25] Stefan Schuhladen, Falko Preller, Richard Rix, Sebastian Petsch, Rudolf Zentel, and Hans Zappe. Iris-like tunable aperture employing liquid-crystal elastomers. *Advanced Materials*, 26(42):7247–7251, 2014.
- [26] Hao Zeng, Owies M Wani, Piotr Wasylczyk, Radosław Kaczmarek, and Arri Priimagi. Self-regulating iris based on light-actuated liquid crystal elastomer. *Advanced Materials*, 2017.
- [27] Owies M Wani, Hao Zeng, and Arri Priimagi. A light-driven artificial flytrap. *Nature Communications*, 8, 2017.
- [28] David B. Hall, Patrick Underhill, and John M. Torkelson. Spin coating of thin and ultrathin polymer films. *Polymer Engineering & Science*, 38(12):2039–2045, 1998.
- [29] qpod® 2e – customizable temperature-controlled sample compartment for use with fiber optic spectrometers. URL: <http://www.qnw.com/qpod-2e/>. Cited: 27.7.2017.
- [30] Yoshimasa Kanawaku, Jun Kanetake, Atsuki Komiya, Shigenao Maruyama, and Masato Funayama. Effects of rounding errors on postmortem temperature measurements caused by thermometer resolution. *International Journal of Legal Medicine*, 121(4):267–273, Jul 2007.